Transdermal Minimally-Invasive Optical Multiplex Detection of Protein Biomarkers by Microneedles-Embedded Nanopillars Array

Adva Raz[1#], Hila Gubi[2#], Adam Cohen[1] and Fernando Patolsky[1,2*]

1. Department of Materials Science and Engineering, the Iby and Aladar Fleischman Faculty of Engineering, Tel Aviv University, Tel Aviv 69978, Israel.
2. School of Chemistry, Faculty of Exact Sciences, Tel Aviv University, Tel Aviv, 69978, Israel.
# Contributed equally.

Emails: fernando@tauex.tau.ac.il

Abstract

Biomarkers detection have become essential in medical diagnostics and early detection of life-threatening diseases. Modern-day medicine relies heavily on painful and invasive tests, the extraction of large volumes of venous blood being the most common tool of biomarker detection. These tests are time-consuming, expansive, and require complex sample manipulations and trained staff. The application of 'intradermal' biosensors utilizing microneedles as a minimally-invasive and pain-free sampling and sensing elements for capillary blood biomarkers detection has gained extensive interest in the past few years as a central point-of-care (POC) detection platform.

Herein, we present a new diagnosis paradigm based on vertically-aligned nanopillars array-embedded microneedles sampling-and-detection elements for the direct optical detection and quantification of biomarkers in capillary blood. We present here the first demonstration on the simple fabrication route for the creation of a multidetection-zone silicon nanopillars array, embedded in microneedle elements, followed by their area-selective chemical modification, towards the multiplex intradermal biomarkers detection. The utilization of the rapid and specific antibody-antigen binding, combined with the intrinsically large sensing area created by the nanopillars array, enables the simultaneous efficient ultrafast and highly sensitive intradermal capillary blood sampling and detection of protein biomarkers of clinical relevance, without requiring the extraction of blood samples for the ex-vivo biomarkers analysis. Through preliminary *in vitro* and *in vivo* experiments, the direct intradermal *in-skin* blood extraction-free platform has demonstrated a remarkable sensitivity (low pM) and specificity for the accurate multiplex detection of protein biomarkers in capillary blood.

Introduction

Biomarkers detection have become an essential tool in medical research and practice, aiding in the diagnosis of diseases, monitoring treatment effectiveness, and identifying potential drug targets. However, modern-day medical diagnostics still faces significant challenges, such as limited sensitivity and specificity, high cost, technical complexity, low sampling-to-detection cycle turnover and more, which can impede their efficacy and practicality in patient care[1–4]. Despite the remarkable advances in medical diagnostics, there is an ongoing enormous need to address these challenges, in order to enhance their applicability in the medical industry. Biomarkers, as quantifiable indicators of biological processes, hold significant potential in providing essential information on the health status of patients. By overcoming these challenges, biomarkers and other diagnostic tools can facilitate more accurate disease diagnosis and personalized treatment strategies.

Traditional laboratory-based procedures for protein biomarker identification can be time-consuming and invasive to acquire a sufficient amount of blood. Moreover, good medical care can be expensive, promotes the risk of infections to the patient or sample hemolysis, and require specialized equipment and skilled personnel [5,6]. These factors make it challenging to implement POC testing using current methods of blood extraction, particularly in resource-limited or remote settings. POC testing tentatively provides an alternate technique, allowing for the detection of protein biomarkers faster, cheaper, and at the patient's bedside or in the doctor's office, even at home settings, without the need for laboratory equipment or specific training [7,8]. Many POC diagnostics rely on the sampling of blood by venepuncture, which is a procedure that requires a healthcare professional and can be painful and uncomfortable for patients [9–11]. The limits of present technologies can be overcome by creating alternative blood extraction-free approaches, such as on-chip nanostructured devices. Furthermore, the simultaneous measurement of multiple bioanalytes in a single sample is highly desirable, offering fast, inexpensive, and reliable quantification. Therefore, applicable multiplexed POC testing which tackles all of the aforementioned challenges has become a major point of interest, and serves as a holy grail for medical diagnostics.

To address these issues, capillary blood sampling has been proposed as a minimally invasive alternative to venepuncture for POC diagnostics. It can be extracted by individuals themselves, which can increase accessibility to testing and eliminate the need for healthcare professionals [12–14]. However, capillary blood samples have been associated with varying biomarker concentrations, which may limit the accuracy and reliability of POC diagnostic tests. Furthermore, numerous issues arise when minimal volumes of bodily fluids are extracted for diagnostic testing, namely, uncontrollable detrimental effects that can occur during extraction and post-extraction manipulation steps, such as clotting and hemolysis [15–17]. These effects can negatively impact the quality and accuracy of the sample, particularly before it reaches the final sensing phase. As a result, it is often not possible to perform multiplexed biomarker

analyses on these small-volume samples, which can impede diagnosis and lead to significant analytical artifacts.

Analyzing capillary blood samples was recently shown to be possible *via* microneedle-based systems due to their direct and minimally-invasive whole-blood extraction approach. As a minimally invasive technique, the microneedle insertion is almost painless and devoid of discomfort, ensuring a positive patient experience during the sampling process. Moreover, the tiny needle minimizes tissue trauma, thereby reducing the likelihood of complications such as hemolysis and the risk of infection throughout their use [18–22]. The direct detection of capillary whole blood can eliminate the need for traditional laboratory equipment for the smaple manipulion and pre-treatments, thereby enhancing healthcare accessibility and facilitating point-of-care testing.

The latest developments include new apparatuses including multiplexed arrays using microelectronics [23], glucose level monitoring in diabetic individuals [24–26], and biomarkers detection in interstitial fluid [27–29] and more [18]. Multiplexed microneedle arrays are engineered to collect multiple biomarkers simultaneously, reducing the number of samples required, while improving diagnostic accuracy making them useful for point-of-care testing. These technological developments have the potential to revolutionize healthcare by allowing for minimally invasive and rapid monitoring of biomarkers in whole capillary blood, leading to earlier disease detection and personalized treatment. Notably, most of the previously mentioned paradigms are microelectronic-based platforms, and can measure changes in the electrical properties of the sensing surface upon biomolecules binding. The major advantage of electronic biosensors is their high sensitivity, rapid response, and good linearity, theoretically allowing for excellent protein detection [19]. However, several disadvantages plague electronic biosensors, making them inadequate for universal applications. Namely, they can be susceptible to signal drift and interference, which can result in inaccurate readings and require frequent calibration. Additionally, electronic biosensors may require complex fabrication and processing, leading to high costs and limited scalability for mass production [30,31].

In this context, optical fluorescence-based biosensors rely on a different approach, utilizing the fluorescence emission of a probe upon interaction with the target molecule. In contrast to electronic biosensors, they offer high sensitivity and selectivity, as well as stability and the ability to detect and quantify a wide range of targets. Fluorescence-based biosensors also have a wide dynamic range, enabling the detection of low-abundance targets in complex biological samples [32,33]. Another advantage of fluorescence biosensors is their compatibility with microfabrication techniques, which allows for the development of miniaturized devices for point-of-care and field-based applications with a simple operation. In contrast, electronic biosensors may be limited by their need for external power sources [34].

In a prior study conducted by our group, the remarkable efficacy of vertical arrays of silicon nanopillars (SiNPs) for the rapid separation and sensing of target proteins from complex bio-samples was

demonstrated [35–37]. The SiNPs platform was created via metal-assisted chemical etching (MACE), to create a stable nanostructured surface directly from a silicon wafer. MACE is a simple and low-cost method for fabricating Si nanostructures with the ability to control their shape, diameter, length, and nanostructure orientation relative to the substrate [38,39]. The SiNPs provides several advantageous features as a sensing area for biosensing applications and especially immunosensors. For example, a high surface area-to-volume ratio renders them highly sensitive to changes in the local environment, a crucial characteristic for detecting small amounts of analytes and enhancing the resulting signal [32,40–42]. Furthermore, the three-dimensional architecture of SiNPs creates organized cavities with limited protein diffusion. This results in a substantially lower mean-free path for the proteins, forcing them to linger inside the cavities as they are being repeatedly adsorbed to the surface-anchored antibodies on the pillar surfaces within the limited inter-pillars region. Hence, improving the accessibility of analytes to the sensing elements, amplifying their sensitivity [35].

Herein, a fully integrated novel array-like device is presented in this work which combines the advantageous architectures of both microneedle-like devices and SiNPs ultra-efficient biomarkers collecting elements as the sensing area. The direct fabrication process of the device results in a fully embedded SiNPs array on the surface of the needles, while each sensing sub-area of the array can be further functionalized with specific antibodies, targeting specific proteins and biomarkers. The needle-embeeded nanopillars array allows direct, rapid and minimally invasive capillary whole-blood sampling, while the sensory area of the functionalized embedded SiNPs serves as an excellent bed for immediate analysis of the sample via fluorescence microscopy. The device's diagnostic clinical capability for highly sensitive, selective multiplex detection of protein biomarkers, such as Prostate specific antigen (PSA), which was selected as a preliminary proof-of-concept candidate, was demonstrated in this study. These findings pave the way for near future applications in the detection and diagnosis of additional biomarkers related various diseases of interest.

Results and Discussion

A silicon microneedle-embedded SiNPs array was created to support the monitoring of physiological parameters through the skin. Intradermal monitoring requires a robust sensing device that will stay stable and functionalized during the implementation [23,43,44]. The fabrication process of the microneedle platform is schematically depicted in **Figure 1a**. A P-type dopant native silicon oxide wafer was selected, with a crystallographic orientation of (100). The crystallographic orientation of the silicon wafer is of paramount importance in creating vertically aligned SiNPs using the anisotropic etching process of the MACE reaction [38,39]. Prior to the fabrication process and in order to prevent damage to the nanostructure, the backside of the needle region undergoes mechanical thinning using a dicing saw. The SiNPs was fabricated by the deposition of a monolayer of polystyrene beads, 500 nm in diameter,

using a spin-coater on the silicon wafer to use as an etching mask for the MACE reaction. In order to reduce the diameter of the beads down to 300 nm, to create a beads array with an inter-distance of 200 nm they were subjected to oxygen plasma etching. The beads were deposited with 45nm of metal silver as a catalyst for the etching reaction while the sensing area was fabricated using standard UV lithography, wet etchers, and oxygen plasma. The vertical SiNPs array is formed using the silver catalyst and HF/H_2O_2 mixture as the etchant and oxidating agent, respectively. The final SiNPs array consists of tens of thousands of pillars with heights ranging from 5-15µm, **Figure S1** depicts a focused ion beam (FIB) cross-section of the fabricated SiNPs after spattering.

To acquire the final structure of the sharp tip microneedle for easy penetration of the skin, a deep reactive ion etching (DRIE) approach was used. The SiNPs structure, together with the thin edge of the needle is prone to high-energy ion damage, which will result in structural defects. The needle region thinning previously presented reduces the etching time and prevents damage. Once the entire device is ready, a SiO_2-protective layer was deposited using plasma-enhanced chemical vapor deposition (PECVD). The silica layer with a thickness of approximately 20 µm was fabricated as a 150 µm X 120 µm pool. Energy-dispersive X-ray spectroscopy (EDS) analysis of the compounds on the surface of the needle is presented in **Figure S2** showing the silicon oxide window around the SiNPs sensing area. Moreover, a scanning electron microscopy (SEM) image using the backscattered electron detector (BSD) is depicted in **Figure S3** shows the shadowing effect surrounding the sensing window, due to the added 20µm of silica. This design was implemented to ensure accessibility to the sensing area while maintaining the integrity of the microneedle region, the silica pool is an important step in the design of a functional microneedle area. The protective layer serves numerous functions, starting with addressing the potential contamination encountered during the penetration of the skin [45]. Additionally, the insertion of the sensing elements into the intradermal layers can result in mechanical abrasion and subsequent detachment of the covalently attached molecular biorecognition layer [20,45,46]. By etching the silicon wafer, the pillars are formed, with their tips positioned at the surface level while being shielded by the bulk of the wafer. Furthermore, the incorporation of several microns of silica provides supplementary safeguarding for the pillars during the insertion process. Hence, the elevation of the surface height *via* the silica layer emerges as an indispensable and pivotal factor for the successful execution of blood extraction-free, intradermal protein detection. The final microneedle-embedded pillars are shown in the SEM image provided in **Figure 1b**, the blue inset represents a higher magnification of the SiNPs sensing area. Within the scope of **Figure 1**, a single sensing area is fabricated on each needle, as depicted in **Figure 1c**. The maximum amount of sensing areas for each needle is solely limited by the dimensions of the needle itself and the desired size of the individual sensing sub-areas. Therefore, the direct fabrication of multiplex devices becomes feasible, thereby enabling enhanced redundancy in sensing capabilities. **Figure 1c** inset illustrates the fabrication of six distinct sensing areas, demonstrating the potential of this platform.

To recive the most effective sensing devices, the exact length of the microneedle element should be determined. Previous work of the group, as well as additional research on that topic, showed that 1000µm microneedle is the optimal needle length to reach and rupture intradermal blood capillaries networks, while maintaining minimal discomfort for patients [23,47].

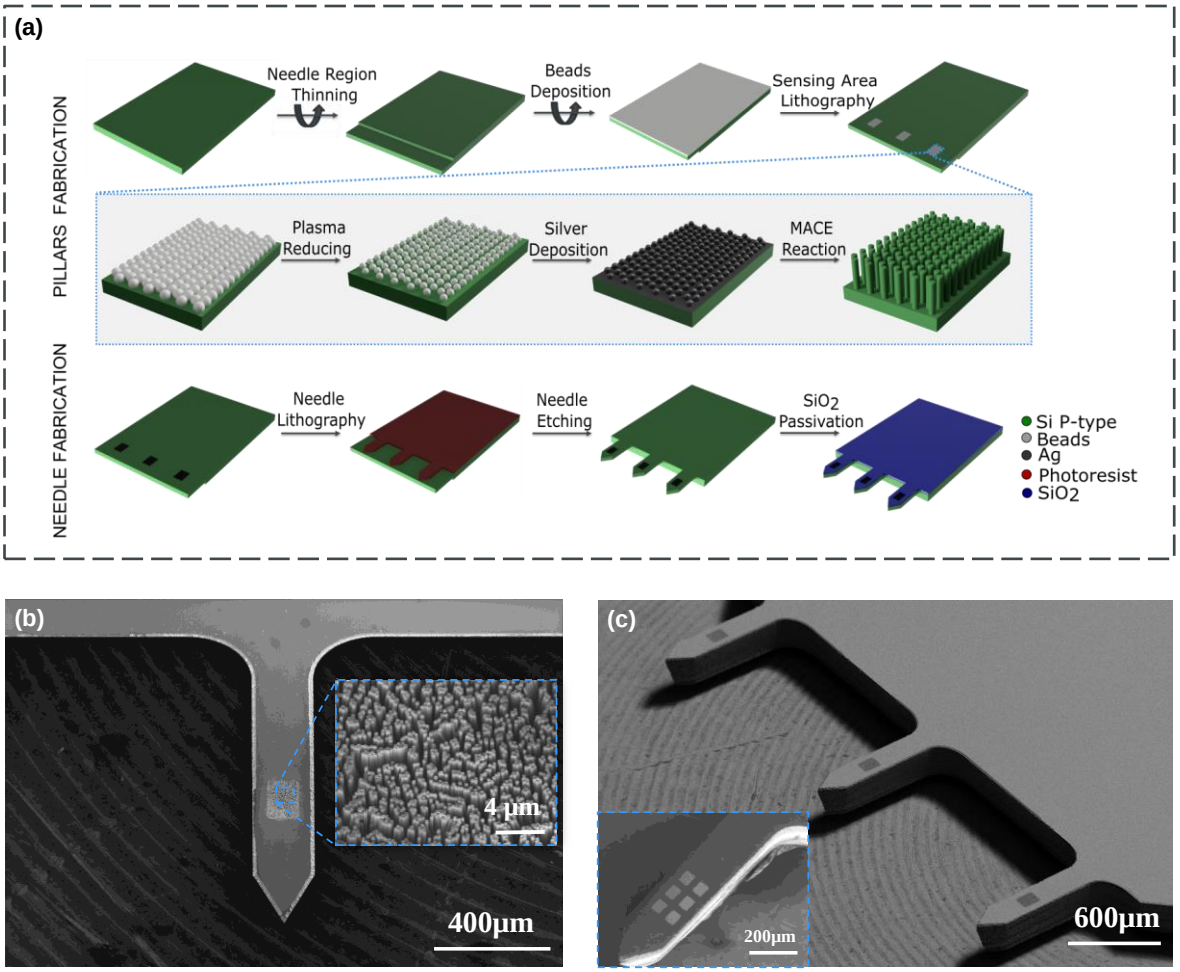

Figure 1 | Fabrication and characterization of the SiNPs-based microneedle array. **(a)** Schematic illustration of the fabrication process. **(b)** SEM images of the fabricated needles with the SiNPs array; the dimensions of the needles are 220 µm in width and 1000 µm in length, while the sensing area is 120 µm and 150 µm respectively. The blue inset shows a higher magnification image of the vertically aligned and ordered SiNPs sensing array. **(c)** SEM imaging of the entire microneedle device presenting the three-needle apparatus, each needle with one sensing area. The blue inset shows an alternative fabrication design including six sensing areas on the needle structure for possible multiplex detection on one needle.

The monitoring and quantification of numerous protein biomarkers is critical for the early identification of a wide spectrum of diseases. Typically, this entails an invasive and unpleasant operation that involves the extraction of a few milliliters of venous blood for diagnostic purposes. Nonetheless, immense progress has paved the way for a potential decrease in the necessity for this procedure. Rapid antibody-

antigen binding followed by fluorometric intensity measurements can be applied with the use of minimal capillary blood samples. This method minimizes invasiveness and discomfort while allowing for quick diagnostic analysis.

As proteins from the human body are mostly non-fluorescent, to first show the ability of the device, a modification of the anti-green fluorescence protein (GFP) antibody was conducted. In order to enable transdermal monitoring of different biomarkers and proteins, a chemical modification of the SiNPs surface is conducted as schematically illustrated in **Figure 2a**. First, the needles were dipped in 3-aminopropyldimethylethoxysilane (APDMES) solution, an amino-silane derivative, for 2 hours in an inert environment. Followed by a thorough wash in toluene and IPA, and placed on a heating plate at 115°C for 30 minutes for full dehydration to fully stabilize and enhance the covalent bonds stability between the APDMES and the surface and evaporate all solvents [48]. Subsequently, the needles were immersed in a solution consisting of 160µL of a 10% glutaraldehyde solution in phosphate buffer containing 50mg of cyanoborohydride, acting as a reduction agent, for the duration of 1 hour followed by a thorough wash in deionized water (DIW). The needles were then modified overnight with 40µg/mL anti-GFP solution in phosphate buffer with 50mg of cyanoborohydride at 4°C. The yield of the binding between the antibody and the glutaraldehyde is low, as some of the glutaraldehyde on the surface remains unbound. To prevent non-specific binding, blocking of unreacted aldehyde was performed by dipping the needles for 2 hours in 160µL of ethanolamine solution (400µL in 25mL phosphate buffer containing 50mg of cyanoborohydride) [49]. An additional 2 hours blocking step is performed by dipping the needle in 160µL of skim milk in phosphate buffer silane (PBS) to minimize non-specific adsorption to the biosensor surface that can interfere with detecting the target analyte [50,51].

X-ray photoelectron spectroscopy (XPS) analysis was conducted for the different modification steps on a silicon wafer with the fabricated SiNPs presented in **Figure 2b**. For the clean silicon wafer, only silicon and oxygen elements from the native oxide layer are observed. Once the APDMES is covalently bonded, a rise in carbon and nitrogen atomic concentration is detected. Furthermore, a significant increase in carbon and nitrogen atomic concentration occurs once the glutaraldehyde and IgG antibody molecules are bonded to the surface. The concentration of silicon and oxygen is reduced in every modification step, as the silicon substrate surface is covered and screened by the introduced organic compounds ad-layers. The XPS measurements show that the antibody modification process to the sensing device was successful. Full XPS spectra are shown in **Figure S4**.

To further show the success of the modification process, the anti-GFP antibody chemically-modified microneedle array was incubated in the precense of the GFP protein. The first needle was dipped in a low concentration of GFP, 10pM, while the second microneedle was incubated in a high concentration of GFP, 10nM. **Figure 2c** presents fluorescence microscopy images, showing the different contrasts in

the images due to the difference in the fluorescence intensity. The microneedle introduced to high GFP concentration shows a high contrast with a high-intensity fluorescence signal from the SiNPs active window, while the second microneedle shows low contrast between the SiNPs active window and its surrounding microneedle surface due to low fluorescence intensity. The different reactions demonstrate the successful antibody-antigen binding, and thus the successful antibody anchoring the the SiNPS active surface, proving the successful chemical modification steps.

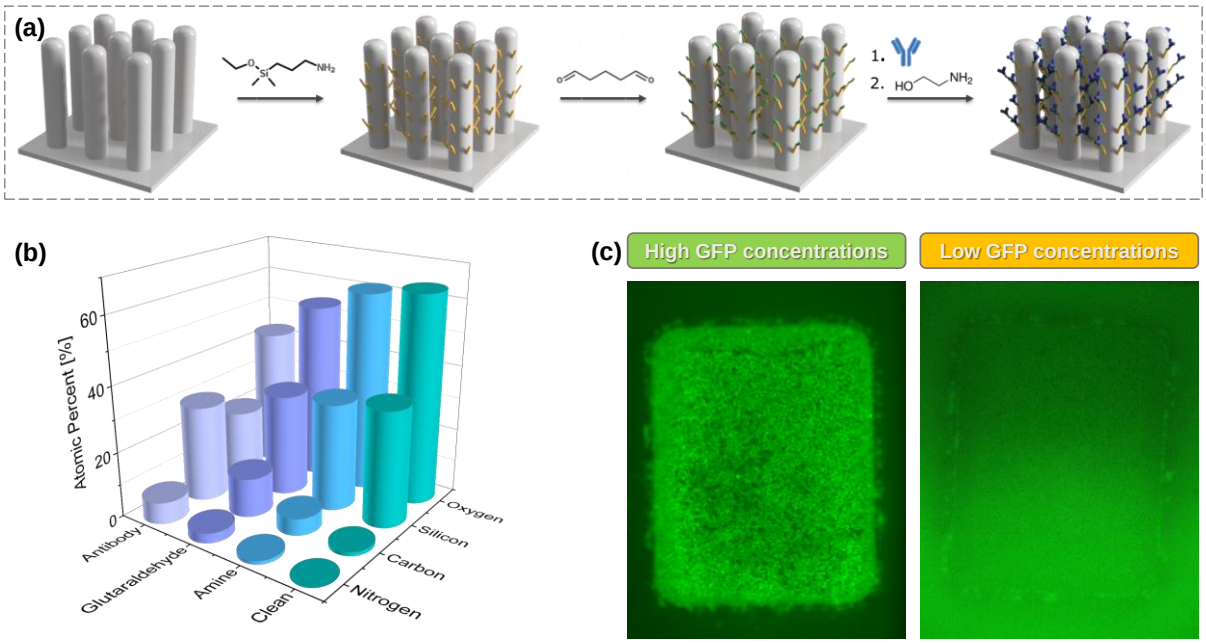

Figure 2 | Surface modification process. **(a)** Schematic illustration of the four steps of the chemical modification process. **(b)** XPS results of the four different stages of surface modification. **(c)** Fluorescent microscopy images showing the concentration-dependent fluorescence intensities as a result of GFP protein binding to the modified surface.

Preliminary fluorescence microscopy experiments were conducted to show a concentration-dependent behavior for the binding of the protein GFP, the samples were excited using a 470nm wavelength, and the fluorescence was measured at an emission range of 495-535nm [52]. **Figure 3a** illustrates the linear response curves to different GFP concentrations in spiked PBS buffer. Similarly, **Figure 3b** represents measurements in bovine serum spiked with rising GFP concentrations. An clear linear increase in the fluorescence intensity was measured as a result of the specific binding of GFP to the surface of the antibody-modified SiNPs-embedded microneedle element. Signal normalization was performed against an unspiked solution. The response is taken as an average value of the entire sensing area. These results show a detection sensitivity and limit of detection (LOD) in the low pM range.

Specificity tests of the microneedle-embedded SiNPs array response were conducted by measurements in the presence of high concentrations of the nonspecific GFP biomarker, as shown in **Figure 3c**. The SiNPs array was modified with anti-Cytochrome C, anti-CA-15-3 and anti-cardiac troponin T (cTnT) antibodies, and showed near to zero response to the introduced highly-concentrated GFP protein. On the other hand, the anti-GFP-modified SiNPs array showed high fluorescence intensity in the presence of the GFP protein. These results indicate the high specificity of our sensing microneedle devices for the specific detection of the desired protein biomarker. This concept is presented in the fluorescence measurements in **Figure 3c** inset. The two microneedles were introduced to the GFP protein solution, while the left needle modified with anti-GFP showed a response to the GFP protein, the right needle modified with anti-cTnT showed no response to the non-specific GFP protein.

The safety and mechanical integrity of the SiNPs sensing area within the silica pool are of utmost importance for the final clinical application of the sensing platform, and were further explored by a series of additional tests. **Figure 3d** presents fluorescence measurements of the microneedles incubated with increasing GFP concentrations, before (cyan dots) and after (purple dots) polydimethylsiloxane (PDMS), a skin-mimicking slab pricking. The plot shows that the fluorescence intensity values do not change as a result of the microneedle insertion into the PDMS block, demonstrating the absence of any mechanical abrasion on the covalently-attached sensing layer during insertion. Moreover, these tests were conducted to provide conclusive evidence regarding the robust protection of the SiNPs array, and to ensure their structural preservation during insertion. **Figure 3e** presents optical images together with a schematic illustration of the insertion and extraction process of the microneedle array. The full insertion process is featured in **Movie S1** in the supporting information, which demonstrates that all three microneedles on the device are fully intact following this process. **Figures 3f** and **3g** depict SEM images before and after the insertion, respectively, proving that there are no structural defects and broken pillars as a result of the insertion step. The insets of both **Figure 3f** and **3g** present higher magnification SEM images of the SiNPs, showing that the PDMS did not leave any residue on the array. Aside from acting as a protection layer for the biorecognition layer, this deposited protective layer creates a 20μm window, allowing fast and full wetting of the sensing area when introduced to the analyzed medium. By pricking, a capillary blood "pool" forms inside the sensing area window [23].
Figure S5 shows the repeatability between three microneedles on a single chip. The plot presents the fluorescence from each needle in response to increasing concentrations of GFP. It is evident that for good coverage of pillars on the sensing area, all three microneedles from the same device react similarly inside the error range. Therefore, the microneedles arrays are highly reliable and produce an extremely reproducible response.

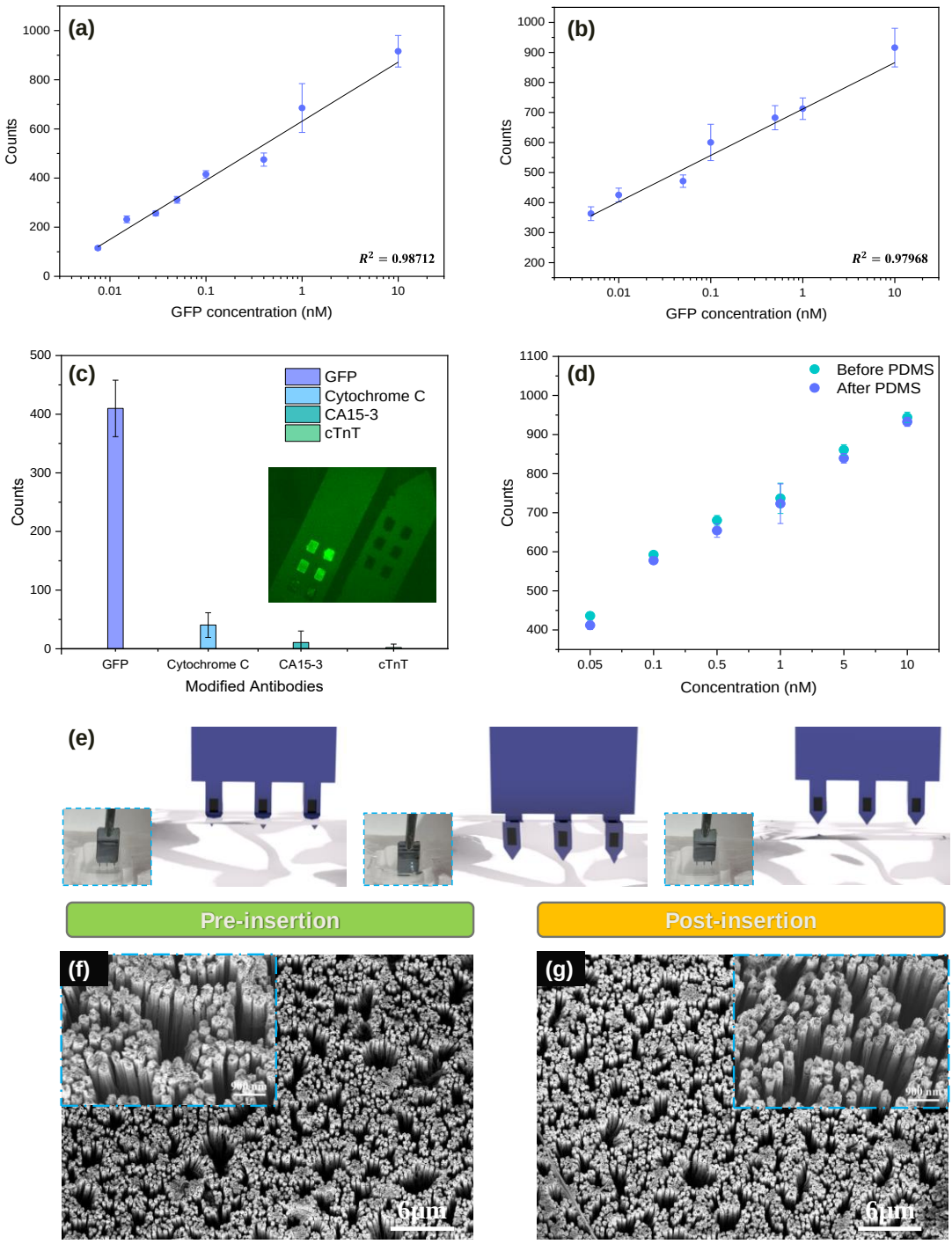

Figure 3 | **(a)** Linear response curve to increasing GFP concentrations in spiked PBS buffer. The intensity reading is the mean of the entire sensing area. The normalized reaction is in comparison to a clean silicon wafer. **(b)** Linear response curve to increasing GFP concentrations in spiked bovine serum. The intensity reading is the mean of the entire sensing area. The normalized reaction is in comparison to a clean silicon wafer. **(c)** Specificity measurements of four needles, each modified with different antibodies: anti-Cytochrome C, anti-CA-15-3, anti-cTnT, and anti-GFP all introduced to GFP protein. The results clearly show that only the needle modified with the specific anti-GFP antibody presents a high fluorescent response, while the non-specific antibody shows a negligible response. The inset shows

an optic image from the fluorescent microscope presenting the difference in fluorescence between the specific and non-specific binding. **(d)** Fluorescence intensity measurements on the microneedle device sensing area before and after PDMS insertion. The result shows similar intensity measurements between the two, proving no abrasion of the biorecognition layer due to the insertion. **(e)** Schematic illustration of the insertion and extraction of the microneedle device from the PDMS. The blue insets show the respective optic images of the same process. **(f)** SEM image of the SiNPs sensing area before pricking of the PDMS. The blue inset shows a higher magnification of the area. **(g)** SEM image of the SiNPs after extraction from the PDMS showing no deformation of the structure. The blue inset presents a higher magnification of the same area, proving that the pillars stay intact.

While the preliminary concept and fluorescence measurements were conducted using GFP, subsequent measurements were done on real human serum samples for quantifying levels of the protein biomarker PSA in blood. Prostate-specific antigen (PSA), a protein biomarker originating from the prostate gland and found in the seminal fluid, has emerged as a pivotal component in the detection of prostate cancer. Elevated PSA levels in the blood can serve as an indication of prostate cancer. Normal PSA levels in healthy men range up to 4 ng/ml with values exceeding this threshold raising concerns about potential prostate cancer [53,54]. Serum PSA levels in females are generally considered negligible, however, breast tissues can also produce PSA. Elevated PSA levels in female serum may be indicative of conditions such as breast cancer, cysts, or fibroadenomas [55,56]. Consequently, the detection of PSA in blood has become an increasingly prominent role in medicine, diagnostics, and scientific research.

Prior to *in vivo* intradermal measurements in capillary blood, the sensitivity of the microneedle device towards the protein biomarker PSA was evaluated through *in vitro* measurements.
A concentration-dependent sensing behavior was observed, **Figure 4a** demonstrates a linear response to different PSA concentrations in spiked untreated bovine serum samples showing sub ng/ml (low pM) sensitivity, with a LOD of 0.2 ng/ml. Additional specificity tests of the SiNPs platform were performed using high concentrations of the nonspecific proteins Cytochrome C, cTnT and BNP as shown in **Figure 4b**. The concentrations were 100 ng/ml for all tested proteins including the PSA, which is a magnitude higher than the physiological PSA level in a healthy human. The anti-PSA-modified array showed near-zero response to the highly concentrated Cytochrome C, cTnT and BNP, indicating the high specificity of the present sensing microneedle device for the specific detection of the PSA target biomarker. Furthermore, these results demonstrated low sensitivity to varying interferents (proteins, nucleic acids, lipids, etc.), as the measurements were conducted in untreated serum.

Following calibration of the sensing device *via in-vitro* measurements, *in-vivo* intradermal sensing measurements were performed on five human volunteers by inserting the microneedle elements into the intradermal space for a short period of only 1 minute. **Figure 4c** depicts the PSA concentration measurements of the tested subjects extrapolated from the device calibration presented in **Figure 4a**. The tested subjects were: Subject A a healthy 25-year-old female, Subject B a healthy 30-year-old male, Subject C a healthy 25-year-old male, Subject D a healthy 28-year-old male and Subject E a healthy 30-year-old male. The results show that the subjects' PSA levels are within the normal healthy range for all male subjects. Very low PSA levels were measured for the female Subject A, lower than the lowest limit of the detection for the device, showed as the horizontal line, since normal PSA levels in healthy females are about 0.002 ng/ml[57]. The accuracy of the PSA levels recorded from the *in vivo* microneedle measurements was further validated by performing the gold-standard PSA-specific enzyme-linked immunosorbent assay (ELISA) using venous blood samples from the same volunteers. The ELISA results depicted in the blue column in **Figure 4c** confirmed that the microneedles array *in vivo* experiments accurately measured the levels of the target PSA biomarker in blood, which remarkably correlates to the ELISA measurements. In addition, these experiments prove the excellent physiological correlation of PSA concentration levels between venous blood and capillary blood samples.

Nowadays new platforms of microneedle devices for POC applications offer the capability for multiplex detection of multiple protein biomarkers in a single test. Each individual needle or sensing area on our device can be modified with a different antibody according to specific requirements. As a proof of concept, a highly accurate micro-dropper (M2 Automation) was employed to label each sensing sub-area on the microneedle device with distinct fluorescent dyes. Specifically, half of the sensing sub-areas were labeled with Alexa Fluor 430, while the other half were labeled with Alexa Fluor 555. Utilizing a fluorescent microscope, the device was initially excited with the corresponding wavelength, implicit in its name to excite the fluorophores, and their emission was observed using a 495-535 nm filter and 575-615 nm filter, respectively. **Figure S6** presents the raw images received during the adquisition. **Figure 4d** presents the results of the multiplex experiment showing the specific fluorescent emission in each sensing area in response to the appropriate excitation.

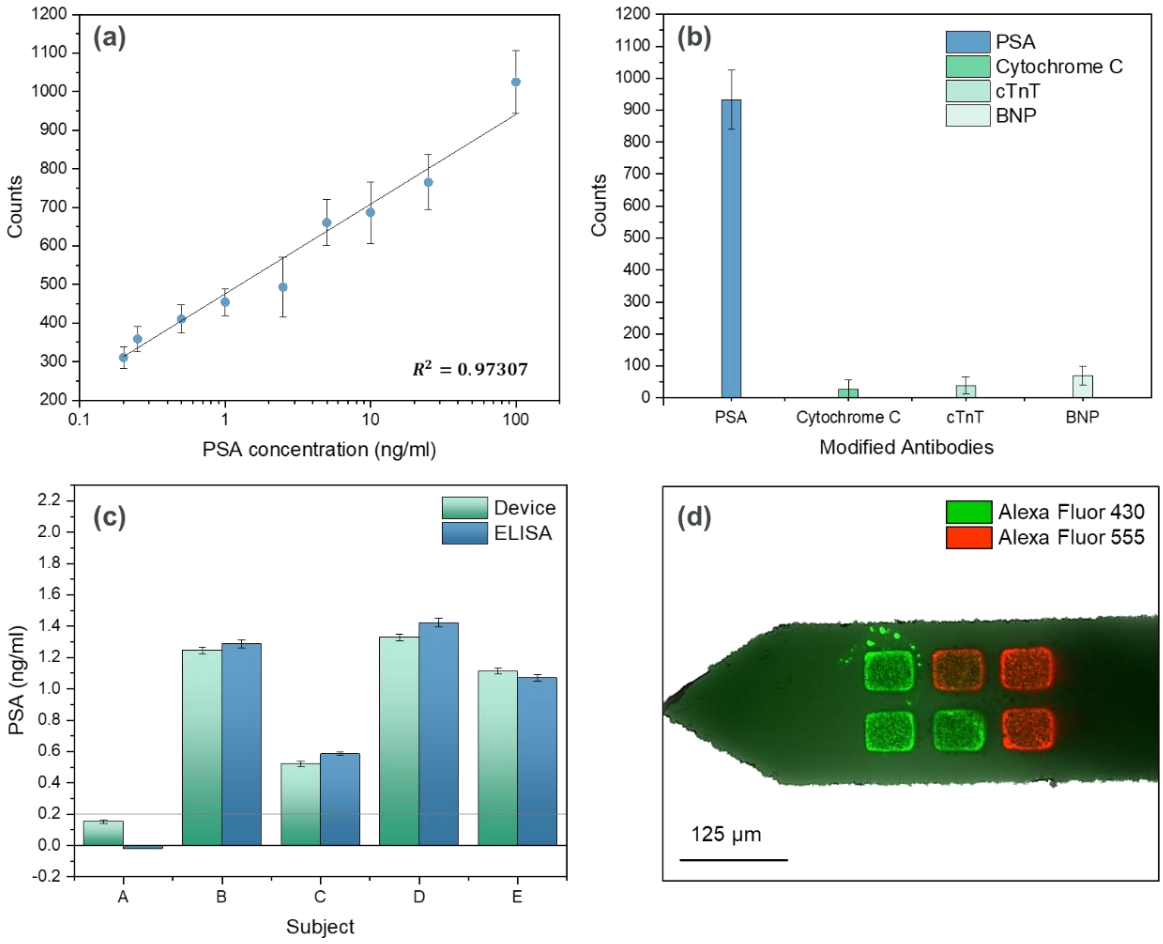

Figure 4 | (a) Linear response curve to increasing PSA concentrations in spiked bovine serum. **(b)** Specificity measurements, each modified with PSA antibody and introduced to different proteins: Cytochrome C, BNP, cTnT, and PSA. The results clearly show that only specific PSA protein biomarker presents a high fluorescent response, while the non-specific proteins show a negligible response. **(c)** *In-vivo* measurements in five volunteers for quantification of PSA concentration using the SiNPs device (cyan bars) in comparison to ELISA measurements (blue bars). (**d)** Fluorescent image of the multiplex detection of two different fluorophores on the multiple sensing area.

For the *in-vivo* measurement, the device was connected to a handle support printed in a 3D printer to facilitate its precise, easy, and stable insertion. **Figures 5a** and **5b** visually depict the skin pricking process before and during the insertion, respectively. Each microneedle on the device serves a crucial function in rupturing the capillary network creating individual blood pools. These blood pools subsequently fill the meticulously designed sensing area within the silica-protected window. **Figure 5c** presents the distinct blood pools generated by each microneedle as a consequence of the skin pricking procedure, each pool corresponds to a specific microneedle on the device chip. **Figure 5d** shows optical microscope images of the microneedle with the silica-protected layer before its contact with a blood

droplet. The microneedle was then introduced to a blood droplet evident by the red blood cells on the microneedle area presented in **Figure 5e**. The device's ability to accurately sense bioanalytes diretly from capillary blood depends on the interface between the sample and the SiNPs array sensing area on the device. **Movie S2** portrays the blood droplet draining into the depressed SiNPs array, fully wetting and saturating the sensing interface.

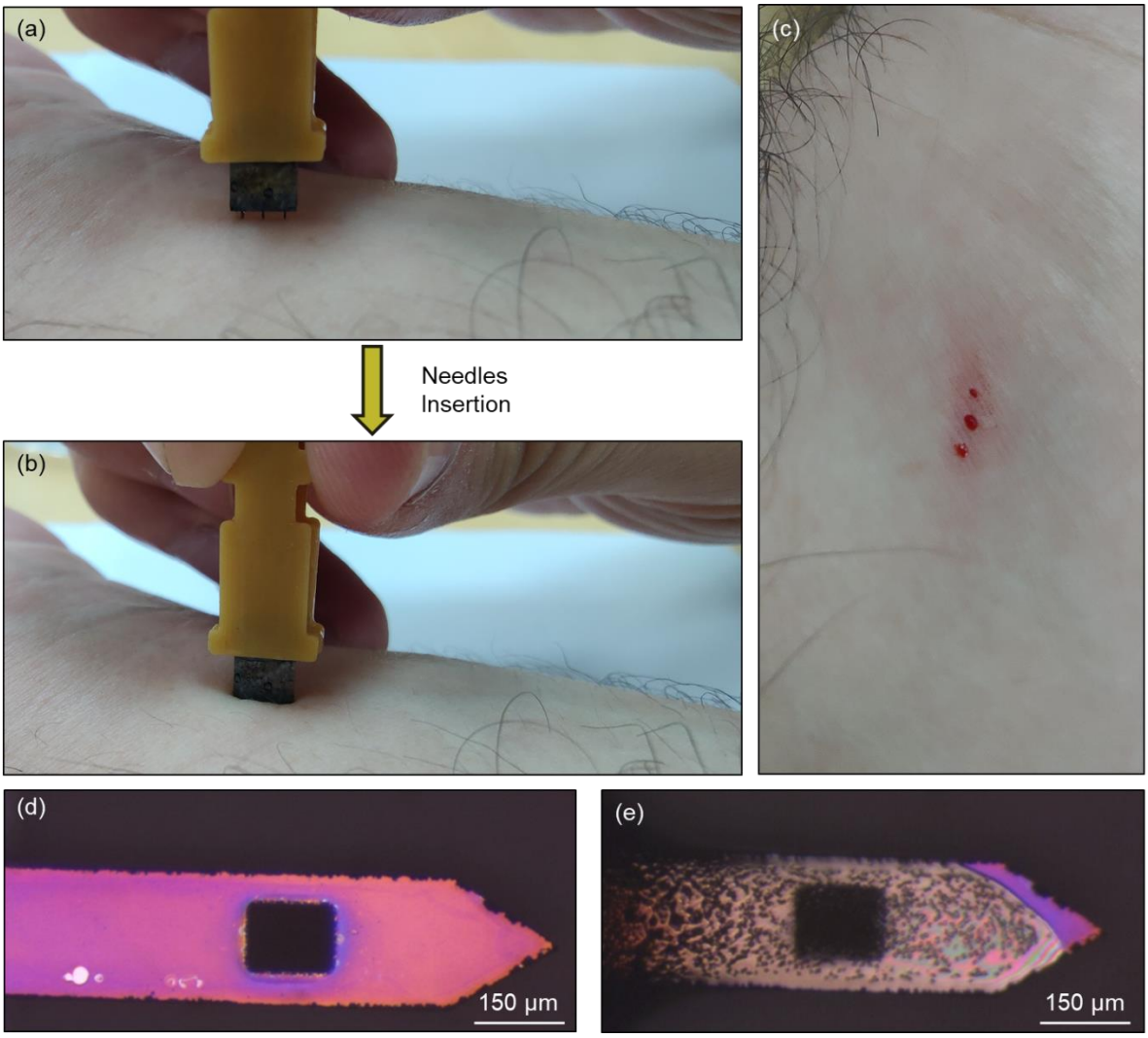

Figure 5 | (a) The initial pricking step of the microneedle device connected to a 3D printed holder **(b)** A fully insertion microneedle device inside a volunteer arm. **(c)** Three puncture holes for three needles on the device, with visible blood droplets as a result of the capillary network rapture during pricking. **(d)** Optical microscope image of the microneedle with the silica protective window before contact with the blood droplet. **(e)** Optical microscope image of the microneedle after contact with the blood droplet showing red blood cells on the needle surface.

The blood extraction-free microneedle sensing platform presented in this study suggests a groundbreaking advancement in medical diagnosis, especially in POC testing. The current medical diagnostics heavily rely on invasive, time-consuming, and expensive procedures involving extensive blood extraction and manipulation, performed by trained professionals. The proposed diagnostic platform presented here utilizes chemically-modified SiNPs-embedded microneedles, enabling intradermal penetration and quantitative sampling and detection of the desired biomarkers directly from capillary blood. This innovative POC paradigm offers minimally invasive, manipulation-free whole blood detection, while exhibiting high sensitivity, specificity, and fast detection turnover, with multiplex capabilities without the need for external power use.

Conclusions

In conclusion, a new microneedle-embedded SiNPs sensing array platform for the intradermal, minimally invasive, and blood extraction-free platform utilizing optical fluorescence measurements for the clinical POC detection of protein biomarkers is here demonstrated. By a fast simple and cost-effective fabrication process, an array of vertically aligned SiNPs sensing areas is achieved by multiplying the surface area by ten-fold, along the inter-pillar biomarker concentration phenomenum, resulting in a highly sensitive intradermal sensing device. For the protection of the biorecognition layer, a silica layer, surrounding the sensing area was implemented. This silica-protecting window allows no abrasion of the bonded antibody recognition layer from the sensing area while smoothly penetrating the skin to the desired depth. Additional durability test show that no structural damage to the SiNPs array or the microneedle itself is observed as a result of the skin pricking process. The microneedle SiNPS-array shows high specificity to the desired specific biomarkers, with a detection sensitivity limit in the low pM range. Moreover, fluorescence microscopy experiments showcase a clear and linear concentration-dependent sensing behavior to the target analytes under the precense of highly abundant non-specific protein potential interferents. Preliminary clinical tests were performed by the intradermal direct *in vivo* blood extraction-free detection of PSA on human volunteers *via* skin pricking. Our new microneedle-embedded SiNPs sensing platform detection measurements correlate remarkably well with the values measured using venous blood from the same volunteers through the use of gold-standard ELISA analysis. Moreover, additional multiplex chemical modification of two different fluorophores on a single microneedle proves the high POC testing abilities of our novel diagnostic method. Future integration of the platform with a portable optical readout system can further enhance the usability of this device, enabling various on-site and real-time clinical diagnostics. By utilizing minimal quantities of in-skin capillary blood, and the rapid antibody-antigen binding coupled with fluorometric intensity measurements, this blood extraction-free microneedle sensing platform holds great promise for improving healthcare outcomes and patient access to advanced diagnostic tools.

Materials and Methods

Materials and Chemicals

For this study, the following materials and chemicals were obtained: polished Si wafer, P-type, (100), 380µm (Silicon Valley Microelectronics), Acetone (9005-68, J.T. Baker), Isopropanol (9079-05, J.T. Baker), Ethanol 97% (Bio-Lab), N-methyl-2-pyrrolidone (NMP, J.T. Baker), Hydrogen peroxide (30% in water, Bio-Lab), Methanol (HPLC, Bio-Lab), Triton X-100 (Sigma-Aldrich), Sulfuric acid (95–98%, Bio-Lab), Buffered oxide etchant 6:1 (BOE, Transene), Hydrofluoric acid (48%, Sigma-Aldrich), Hydrochloric Acid (32%, Bio-Lab), Gold etchant TFE (Transene), Micro particles based on polystyrene (500nm, 10% in DIW, Sigma-Aldrich), AZ-1518 (MicroChemicals), AZ-1505 (MicroChemicals), AZ-726 (MicroChemicals), PR1-12000A1 (FUTURREX), RD6 developer (FUTURREX), Heatsink grease (Dow Corning 340 Heat Sink Compound Grease), Deionized water (18 MΩ·cm), Phosphate buffer (PB, 10 mM, pH 8.5), Phosphate buffer saline (PBS, 10 mM, pH 7.4, with 2.7 mM KCl and 137 mM NaCl, Sigma-Aldrich), Glutaraldehyde solution (50 wt % in H2O, G7651, Sigma-Aldrich), Sodium cyanoborohydride (Angene), Ethanolamine (98%, Sigma-Aldrich), (3-aminopropyl)-dimethyl-ethoxysilane (APDMES, 18306-79-1, Angene), Anti cardiac troponin T antibody (F24T19, HyTest), GFP protein (ab84191, ABCAM), Anti-GFP antibody (ab1218, ABCAM), Zeba spin desalting columns (Thermo scientific), Anti-CA15-3 antibody (Alpha Diognistic), Anti-Cytochrome C antibody (ab76237, ABCAM), Dry skim milk powder (LAB-M), PDMS (Sylgard), PSA antibody pair (ab256313, ABCAM), PSA protein (ab78528, ABCAM) , BNP protein (ab87200, ABCAM), cardiac troponin T protein (ab209813, ABCAM), Human Cytochrome C (ab131847. ABCAM), Alexa Flour 647 (A-20186, Thermo-Fisher), Alexa Fluor 430 (A-10169,Thermo-Fisher), Alexa Fluor 555 (A-37571, Thermo-Fisher) , Human PSA ELISA Kit (ab264615, ABCAM).

Preparations of the Silicon Wafer

To prepare the silicon wafer for the needles and pillars fabrication, AZ-1505 resist was dispensed and spin-coated (500 rpm for 5 s and 4000 rpm for 45s) on the wafer for protection during the dicing process. A 3-inch p-type wafer was diced into 30X30 mm pieces using an automatic dicing saw (Disco DAD 3350). For the thinning of the needle area, AZ1505 was spin-coated again on the front side of the silicon die, as the dicing was done on the backside. The dies were thinned on the intended needle areas to approximately 250µm by lowering the saw up to the desired depth.

Nanopillars Fabrication

First, a premade 400:1 methanol-triton X solution was added to the polystyrene bead solution to create 1.3% polystyrene bead suspension, followed by the addition of 5% volume of ethanol (97%) to the mixture. The suspension was dispersed by shaking for 10 minutes using a vortex. The 30X30 mm dies were thoroughly cleaned with acetone to remove all resist residues, followed by immersing in fresh

piranha solution (H_2O_2 30%:H_2SO_4, 1:3) for 5 min, and a thorough washed with DIW and drying using an N_2 gun. The surface was additionally cleaned and oxidized using an O2 Plasma generator (100 W 10 min).

The polystyrene beads suspension was spread evenly by dispensing 90µL of the solution on the cleaned substrate and spin-coated (100 rpm for 60s, 280 rpm for 35s, 700 rpm for 40s, 1200 rpm for 15s). The polystyrene beads size was reduced to 300nm diameter using PECVD plasma etching (50 sccm O_2, 40 mTorr, 30W, 7 min). A 45nm of silver film was thermally deposited onto the surface (0.2Å/s).

For the fabrication of the desired sensing areas on the device, the silver and beads were removed using lithography techniques, leaving only the necessary sensor regions covered and protected. AZ-1518 photoresist was spin-coated and baked with the same parameters as before and exposed to a UV light with a dose of 45mJ/cm^2. The substrate was developed in AZ-726 developer for 1 min, and silver and beads were removed from the unwanted areas using gold etchant (TFE) for 30s and O_2 plasma etching (50 sccm O_2, 40 mTorr, 30W, 15 min) respectively.

The SiNPs formation was accomplished by wet etching the silicon substrate in an 8 mL solution of 7.6M HF and 0.29M H_2O_2 in DIW for 15 minutes followed by a thorough wash in DIW. Residues of silver and polystyrene beads were removed with HNO_3 and O_2 plasma respectively (50 sccm O2, 40 mTorr, 30W, 15 min).

After the needle formation in the DRIE, a protective passivation layer of SiO_2 was deposited on the microneedle device leaving the sensing area clean. In order to protect the sensing area from the passivation, AZ -1518 photoresist was spin-coated and baked with the same parameters as before and exposed to a UV light with a dose of 45mJ/cm^2. The substrate was developed in AZ-726 developer for 1 minute and the microneedle was placed inside the PECVD for the deposition. (140 sccm N_2O, 40 sccm 2% SiH_4/Ar, 80°C, 95 mTorr, 30 W bias 200W ICP , 1h))

Needle Fabrication

To protect the fabricated SiNPs from possible damage, a thick resist was applied before the deep reactive ion etching procedure (DRIE, Deep RIE Versaline DSE). PR1-12000A1 resist was applied and spin-coated at 300 rpm for 10 s and 3000 rpm for 40s, then baked at 120°C for 3 min. The etch mask was exposed to 480mJ/cm^2 divided into 5 short and consecutive exposures. Following exposure, the die was placed in RD6 developer for 8 minutes under constant rotation. BOE solution was used to remove the oxide layer from the unprotected silicon area. The substrate was then placed in the DRIE and etched for 150 loops. The die was separated into individual devices using the dicing saw and placed in warm NMP to remove the remaining resist.

Antibody Modification

Before the modification process, the microneedle device was placed in the PECVD for 15 minutes (200 sccm O_2, 260mTorr, 100W) to remove all carbon content from the surface and to generate silanol groups on the SiNPs. In a glovebox under an Ar atmosphere, the device was placed in 200µL of 95% APDMES solution for 2h. The device was then submerged in 160µL of toluene to remove any remaining APDMES solution, extensively washed with IPA, and heated at 115°C for 30 minutes to completely evaporate any remaining solvents and to fully stabilize and enhance the covalent bonds between the APDMES and the surface.

Phosphate buffer (PB) was prepared by mixing 10mM potassium phosphate monobasic solutions and 10mM potassium phosphate dibasic solutions to pH 8.5. To bind the second linker, glutaraldehyde, 5mL of filtered PB (FPB) with 50mg of sodium cyanoborohydride was mixed with 1mL of a 50% glutaraldehyde solution. The device was dipped in 160µL of the prepared solution for 1 hour and was consecutively rinsed with DIW.

The selected antibody was centrifuged in a desalting column to clean and purify it properly and was consequently diluted to 40µg/mL for the modification using a prepared solution of 5mL of FPB containing 50mg of sodium cyanoborohydride. The microneedle array was dipped in 160µL of the antibody solution and placed at 4°C overnight on the SiNPs device.

A blocking solution was prepared by adding 100mM ethanolamine to FPB with 50mg of sodium cyanoborohydride, followed by a titration to maintain pH 8.5 using HCl 32%. The unreacted aldehyde groups on the SiNPs were then blocked for 2 hours using 160µL of the mentioned solution. The sensor was then thoroughly washed by placing it in a 160µL solution of clean FPB for 15 min. The final antibody modification step was the submergence of the device in a skim milk solution to eliminate all unspecified binding sites. This method was used to modify all the antibodies used in this study.

***In Vitro* and *In Vivo* Fluorescence Measurements**

The in vitro measurements took place either in filtered phosphate-buffered saline (FPBS) or bovine serum. The microneedle device was placed inside an eppendorf containing 160µL of either unspiked ("clean") or protein-spiked solutions using different concentrations for approximately 1 hour. The measurements were conducted using a fluorescence microscope with a 470nm LED and a 495-535nm filter (LEICA MD4000M Fluorescence microscope with LEICA DFC450 camera.).

PSA *in* vitro and *in vivo* measurements were done using Alexa Flour dyes. Following the capture antibody modification, the device was placed in 160µL of bovine serum solution with different PSA protein concentrations. Consequently, the device was bound to 160µl of PSA detector antibody previously labeled with Alexa Fluor 647 for 1 hour and thoroughly washed in FPBS to remove the

access antibody. The fluorescence intensity was measured using the fluorescence microscope with a 640 nm LED and a 495-535nm filter.

In vivo measurements in capillary blood were performed similarly to the *in vitro* measurements replacing the spiked protein solution with a full penetration of the microneedle array into the volunteer's skin with a 1 minute wait inside the skin before removal.

Alexa Labeling

PSA antibody-pair was used for the PSA detection (ab256313). The detector antibody was labeled using an Alexa Flour 647 labeling kit (A-20186). 100µL of the detector antibody is added to the given Alexa and incubated for 2 hours at room temperature with a gentle invention of the vial every 15 minutes to fully dissolve the dye. The purification steps involve the removal of unbounded Alexa's to the antibody. Placing a spin column in a 15 ml tube, after stirring the purification resin,1.5 ml of the suspension was added into the column and allowed to settle by gravity. The spin column was placed in the provided collection tubes and centrifuge for 3 minutes at 4000 rpm. 100 µL of the antibody bound to the Alexa was added to the center of the spin column, allowing the solution to absorb into the resin bed. the spin column was placed in an empty collection tube and centrifuged for 5 minutes at 4000 rpm. A small amount of the purified conjugate was diluted using 2ml FPBS.

The sensor was modified with the capture antibody as described above (section 5.2.4). After introducing the device with the PSA protein, the detector antibody labeled with Alexa was incubated at 160 µL for 1 hour.

ELISA Measurements

ELISA kit to quantify total PSA was purchased from ABCAM (ab264615). The measurement protocol is as follows:

A 96-well plate coated with an antibody specific to Human PSA was used. A standard PSA solution of 80,000 pg/ml was diluted in Sample Diluent NS to perform calibration curve measurements of 62.5-4000 pg/ml as shown in Figure S7. The antibody cocktail was prepared using 300 µL 10X Capture Antibody and 300 µL 10X Detector Antibody with 2.4 mL Antibody Diluent 4BI and mixing thoroughly and gently. 50 µl of standard solutions and samples were pipetted into the wells together with 50 µl of the antibody cocktail incubating for 1 hour at room temperature on a plate shaker. The wells were washed thoroughly using 10% wash buffer PT, and then 100µl of TMP development solution was added to each well for 15 minutes in the dark shaking, developing a blue color in proportion to the amount of PSA bound. 100 µl of Stop Solution changes the color from blue to yellow, and the intensity of the color is measured at 450 nm.

Venous blood was extracted and centrifuged to coagulate and remove the red blood cells. The test was performed directly on the separated plasma fluid remaining after diluting by a 4-fold in Sample Diluent NS provided in the kit.

Material Characterization

Microscopy and EDS images were taken using HR-SEM (Gemini 300, Zeiss). XPS measurements were carried out using utilizing a Scanning 5600 AES/XPS multi-technique system (PHI, USA). The SiNPs cross-section images were taken by ion sputtering the sample using ThermoFisher Helios 5 UC focused ion beam system (FIB).

Acknowledgments

The authors acknowledge Dr. Pini Shekter for his XPS analysis, and Mr. Atzmon Vakahi for his help with the cross-section preparation using FIB. For the blood extractions studies, the authors would like to acknowledge Mr. David Peled.

Notes

The research presented here complies with all relevant ethical regulations of the Tel Aviv University Ethics Committee. The human study protocol IRB 71.19.

References

1. Swierczewska, M., Liu, G., Lee, S. & Chen, X. High-sensitivity nanosensors for biomarker detectionw. *Chem. Soc. Rev* **41**, 2641–2655 (2012).
2. Nimse, S. B., Sonawane, M. D., Song, K.-S. & Kim, T. Analyst CRITICAL REVIEW Biomarker detection technologies and future directions. *Analyst* **141**, 740 (2016).
3. Campuzano, S., Pedrero, M., Yáñez-Sedeño, P. & Pingarrón, J. M. New challenges in point of care electrochemical detection of clinical biomarkers. *Sensors Actuators B Chem.* **345**, 130349 (2021).
4. Gao, X., Boryczka, J., Kasani, S. & Wu, N. Enabling Direct Protein Detection in a Drop of Whole Blood with an 'On-Strip' Plasma Separation Unit in a Paper-Based Lateral Flow Strip. *Cite This Anal. Chem* **93**, 1326–1332 (2021).
5. Heireman, L. *et al.* Causes, consequences and management of sample hemolysis in the clinical laboratory. *Clin. Biochem.* **50**, 1317–1322 (2017).
6. Giavarina, D. & Lippi, G. Blood venous sample collection: Recommendations overview and a checklist to improve quality. *Clin. Biochem.* **50**, 568–473 (2017).
7. Wang, C. *et al.* Point-of-care diagnostics for infectious diseases: From methods to devices.

Nano Today **37**, 101092 (2021).

8. Luppa, P. B., Müller, C., Schlichtiger, A. & Schlebusch, H. Point-of-care testing (POCT): Current techniques and future perspectives. *TrAC Trends Anal. Chem.* **30**, 887–898 (2011).
9. Rey Gomez, L. M., Hirani, R., Care, A., Inglis, D. W. & Wang, Y. Emerging Microfluidic Devices for Sample Preparation of Undiluted Whole Blood to Enable the Detection of Biomarkers. *ACS Sensors* **8**, 1404–1421 (2022).
10. Guo, Q. *et al.* Covalent organic framework-gold nanoparticle heterostructures amplified dynamic light scattering immunosensor for ultrasensitive detection of NT-proBNP in whole blood. *Sensors Actuators B Chem.* **364**, 131872 (2022).
11. Diamond, S. L. & Rossi, J. M. Point of care whole blood microfluidics for detecting and managing thrombotic and bleeding risks. *Lab Chip* **21**, 3667–3674 (2021).
12. Kemper, D. W. *et al.* Analytical evaluation of a new point of care system for measuring cardiac Troponin I. *Clin. Biochem.* **50**, 174–180 (2017).
13. Wu, C. C. *et al.* Evaluation of a rapid quantitative determination method of PSA concentration with gold immunochromatographic strips Urological Oncology. *BMC Urol.* **15**, 1–7 (2015).
14. Verrinder, E. *et al.* Electrochemical Detection of Morphine in Untreated Human Capillary Whole Blood. *ACS Omega* **6**, 11563–11569 (2021).
15. Effenberger-Neidnicht, K. & Hartmann, M. Mechanisms of Hemolysis During Sepsis. *Inflamm. 2018 415* **41**, 1569–1581 (2018).
16. Kupke, I. R., Kather, B. & Zeugner, S. On the composition of capillary and venous blood serum. *Clin. Chim. Acta* **112**, 177–185 (1981).
17. Tang, R. *et al.* Capillary blood for point-of-care testing. *Crit. Rev. Clin. Lab. Sci.* **54**, 294–308 (2017).
18. Xu, N. *et al.* Microneedle-Based Technology: Toward Minimally Invasive Disease Diagnostics. *Adv. Mater. Technol.* **7**, 1–19 (2022).
19. Wang, J. *et al.* Microneedle-based transdermal detection and sensing devices. *Lab Chip* **23**, 869–887 (2023).
20. Dixon, R. V. *et al.* Microneedle-based devices for point-of-care infectious disease diagnostics. *Acta Pharm. Sin. B* **11**, 2344–2361 (2021).
21. Bal, S. M., Caussin, J., Pavel, S. & Bouwstra, J. A. In vivo assessment of safety of microneedle arrays in human skin. *Eur. J. Pharm. Sci.* **35**, 193–202 (2008).
22. Noh, Y. W. *et al.* In vitro characterization of the invasiveness of polymer microneedle against skin. *Int. J. Pharm.* **397**, 201–205 (2010).
23. Harpak, N., Borberg, E., Raz, A. & Patolsky, F. The 'bloodless' Blood Test: Intradermal Prick Nanoelectronics for the Blood Extraction-Free Multiplex Detection of Protein Biomarkers. *ACS Nano* **16**, 13800–13813 (2022).
24. Heifler, O. *et al.* Clinic-on-a-Needle Array toward Future Minimally Invasive Wearable

Artificial Pancreas Applications. *ACS Nano* **15**, 12019–12033 (2021).

25. Dervisevic, M. *et al.* Transdermal Electrochemical Monitoring of Glucose via High-Density Silicon Microneedle Array Patch. *Adv. Funct. Mater.* **32**, 1–10 (2022).
26. Cheng, Y. *et al.* A touch-actuated glucose sensor fully integrated with microneedle array and reverse iontophoresis for diabetes monitoring. *Biosens. Bioelectron.* **203**, 114026 (2022).
27. Wang, Z. *et al.* Microneedle patch for the ultrasensitive quantification of protein biomarkers in interstitial fluid. *Nat. Biomed. Eng.* **5**, 64–76 (2021).
28. Zhang, X., Chen, G., Bian, F., Cai, L. & Zhao, Y. Encoded Microneedle Arrays for Detection of Skin Interstitial Fluid Biomarkers. *Adv. Mater.* **31**, 1–8 (2019).
29. Samant, P. P. *et al.* Sampling interstitial fluid from human skin using a microneedle patch. *Sci. Transl. Med.* **12**, 1–16 (2020).
30. Cai, X. *et al.* Ratiometric electrochemical immunoassay based on internal reference value for reproducible and sensitive detection of tumor marker. *Biosens. Bioelectron.* **81**, 173–180 (2016).
31. Sun, H., Zheng, Y., Shi, G., Haick, H. & Zhang, M. Wearable Clinic: From Microneedle-Based Sensors to Next-Generation Healthcare Platforms. *Small* **2207539**, 1–23 (2023).
32. Huang, J., Wei, F., Cui, Y., Hou, L. & Lin, T. Fluorescence immunosensor based on functional nanomaterials and its application in tumor biomarker detection. *RSC Adv.* **12**, 31369–31379 (2022).
33. Li, Y. *et al.* Highly sensitive fluorescent immunosensor for detection of influenza virus based on Ag autocatalysis. *Biosens. Bioelectron.* **54**, 358–364 (2014).
34. Jia, B. *et al.* Development of a quantum dot nanobead-based fluorescent strip immunosensor for on-site detection of aflatoxin B1 in lotus seeds. *Food Chem.* **356**, 129614 (2021).
35. Borberg, E., Pashko, S., Koren, V., Burstein, L. & Patolsky, F. Depletion of Highly Abundant Protein Species from Biosamples by the Use of a Branched Silicon Nanopillar On-Chip Platform. *Anal. Chem* **93**, 14527–14536 (2021).
36. Borberg, E. *et al.* Light-Controlled Selective Collection-and-Release of Biomolecules by an On-Chip Nanostructured Device. *Nano Lett.* **19**, 5868–5878 (2019).
37. Krivitsky, V. *et al.* Si Nanowires Forest-Based On-Chip Biomolecular Filtering, Separation and Preconcentration Devices: Nanowires Do it All. *Nano Lett* **12**, 4748–4756 (2012).
38. Huang, Z., Geyer, N., Werner, P., De Boor, J. & Gösele, U. Metal-assisted chemical etching of silicon: A review. *Adv. Mater.* **23**, 285–308 (2011).
39. Lai, R. A., Hymel, T. M., Narasimhan, V. K. & Cui, Y. Schottky Barrier Catalysis Mechanism in Metal-Assisted Chemical Etching of Silicon. *ACS Appl. Mater. Interfaces* **8**, 8875–8879 (2016).
40. Murthy, B. R., Ng, J. K. K., Selamat, E. S., Balasubramanian, N. & Liu, W. T. Silicon nanopillar substrates for enhancing signal intensity in DNA microarrays. *Biosens. Bioelectron.*

24, 723–728 (2008).

41. Welch, E. C., Powell, J. M., Clevinger, T. B., Fairman, A. E. & Shukla, A. Advances in Biosensors and Diagnostic Technologies Using Nanostructures and Nanomaterials. *Adv. Funct. Mater.* **31**, 1–38 (2021).
42. Dong, T., Matos Pires, N. M., Yang, Z. & Jiang, Z. Advances in Electrochemical Biosensors Based on Nanomaterials for Protein Biomarker Detection in Saliva. *Adv. Sci.* **10**, 2205429 (2023).
43. Ranamukhaarachchi, S. A. & Stoeber, B. Determining the factors affecting dynamic insertion of microneedles into skin. *Biomed. Microdevices* **21**, 1–8 (2019).
44. Jiang, S., Li, P., Yu, Y., Liu, J. & Yang, Z. Experimental study of needle-tissue interaction forces: Effect of needle geometries, insertion methods and tissue characteristics. *J. Biomech.* **47**, 3344–3353 (2014).
45. Teymourian, H., Tehrani, F., Mahato, K. & Wang, J. Lab under the Skin: Microneedle Based Wearable Devices. *Adv. Healthc. Mater.* **10**, 2002255 (2021).
46. Liu, G. S. *et al.* Microneedles for transdermal diagnostics: Recent advances and new horizons. *Biomaterials* **232**, 119740 (2020).
47. Blicharz, T. M. *et al.* Microneedle-based device for the one-step painless collection of capillary blood samples. *Nat. Biomed. Eng.* **2**, 151–157 (2018).
48. Riazi, H. *et al.* Surface Modification of a MXene by an Aminosilane Coupling Agent. *Adv. Mater. Interfaces* **7**, 1–8 (2020).
49. Frederix, F. *et al.* Reduced nonspecific adsorption on covalently immobilized protein surfaces using poly(ethylene oxide) containing blocking agents. *J. Biochem. Biophys. Methods* **58**, 67–74 (2004).
50. Bañuls, M. J., Puchades, R. & Maquieira, Á. Chemical surface modifications for the development of silicon-based label-free integrated optical (IO) biosensors: A review. *Anal. Chim. Acta* **777**, 1–16 (2013).
51. Contreras-Naranjo, J. E. & Aguilar, O. Suppressing non-specific binding of proteins onto electrode surfaces in the development of electrochemical immunosensors. *Biosensors* **9**, (2019).
52. Pédelacq, J. D., Cabantous, S., Tran, T., Terwilliger, T. C. & Waldo, G. S. Engineering and characterization of a superfolder green fluorescent protein. *Nat. Biotechnol.* **24**, 79–88 (2006).
53. Palsdottir, T. *et al.* The impact of different prostate-specific antigen (PSA) testing intervals on Gleason score at diagnosis and the risk of experiencing false-positive biopsy recommendations: a population-based cohort study. *BMJ Open* **9**, (2019).
54. Chang, H. *et al.* PSA Detection with Femtomolar Sensitivity and a Broad Dynamic Range Using SERS Nanoprobes and an Area-Scanning Method. *ACS Sensors* **1**, 645–649 (2016).
55. Borchert, G. H., Giai, M. & Diamandis, E. P. Elevated levels of prostate-specific antigen in

serum of women with fibroadenomas and breast cysts. *J. Natl. Cancer Inst.* **89**, 587–588 (1997).

56. Black, M. H. *et al.* Serum total and free prostate-specific antigen for breast cancer diagnosis in women. *Clin. Cancer Res.* **6**, 467–473 (2000).

57. Mashkoor, F. C., Al-Asadi, J. N. & Al-Naama, L. M. Serum level of prostate-specific antigen (PSA) in women with breast cancer. *Cancer Epidemiol.* **37**, 613–618 (2013).